JACS
JOURNAL OF THE AMERICAN CHEMICAL SOCIETY
Article
pubs.acs.org/JACS

Spectroscopic Analysis of Catalytic Water Oxidation by $[Ru^{II}(bpy)(tpy)H_2O]^{2+}$ Suggests That Ru^{V}=O Is Not a Rate-Limiting Intermediate

Yulia Pushkar,*[,†] Dooshaye Moonshiram,[†,§] Vatsal Purohit,[†] Lifen Yan,[†] and Igor Alperovich[†,‡]

[†]Department of Physics, Purdue University, 525 Northwestern Avenue, West Lafayette, Indiana 47907, United States

[‡]Research Center for Nanoscale Structure of Matter, Southern Federal University, 5 Zorge Street, 344090 Rostov-on-Don, Russian Federation

Supporting Information

ABSTRACT: Modern chemistry's grand challenge is to significantly improve catalysts for water splitting. Further progress requires detailed spectroscopic and computational characterization of catalytic mechanisms. We analyzed one of the most studied homogeneous single-site Ru catalysts, $[Ru^{II}(bpy)(tpy)H_2O]^{2+}$ (where bpy = 2,2′-bipyridine, tpy = 2,2′;6′,2″-terpyridine). Our results reveal that the $[Ru^{V}(bpy)(tpy)=O]^{3+}$ intermediate, reportedly detected in catalytic mixtures as a rate-limiting intermediate in water activation, is not present as such. Using a combination of electron paramagnetic resonance (EPR) and X-ray absorption spectroscopy, we demonstrate that 95% of the Ru complex in the catalytic steady state is of the form $[Ru^{IV}(bpy)(tpy)=O]^{2+}$. $[Ru^{V}(bpy)(tpy)=O]^{3+}$ was not observed, and according to density functional theory (DFT) analysis, it might be thermodynamically inaccessible at our experimental conditions. A reaction product with unique EPR spectrum was detected in reaction mixtures at about 5% and assigned to Ru^{III}-peroxo species with (−OOH or −OO− ligands). We also analyzed the $[Ru^{II}(bpy)(tpy)Cl]^{+}$ catalyst precursor and confirmed that this molecule is not a catalyst and its oxidation past Ru^{III} state is impeded by a lack of proton-coupled electron transfer. Ru−Cl exchange with water is required to form active catalysts with the Ru−H_2O fragment. $[Ru^{II}(bpy)(tpy)H_2O]^{2+}$ is the simplest representative of a larger class of water oxidation catalysts with neutral, nitrogen containing heterocycles. We expect this class of catalysts to work mechanistically in a similar fashion via $[Ru^{IV}(bpy)(tpy)=O]^{2+}$ intermediate unless more electronegative (oxygen containing) ligands are introduced in the Ru coordination sphere, allowing the formation of more oxidized Ru^{V} intermediate.

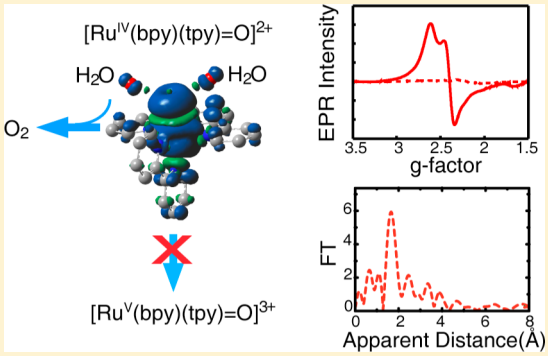

1. INTRODUCTION

To meet society's urgent energy demands, it is important to develop efficient solar to fuel conversion schemes. Mimicking the water oxidation that occurs during natural photosynthesis in a man-made device will provide electrons and protons for the production of chemical fuels. Understanding the mechanism is important for practical realization of light-driven water splitting to H_2 and O_2. Several photoelectrochemical cells (PECs) based on water splitting have been reported recently.[1−3] However, the efficiency and durability of these cells need to significantly improve to become viable energy solutions.

Molecular catalysts of water oxidation allow for catalyst design via ligand substitution as well as provide a convenient system for mechanistic analysis. Recently, molecular catalysts have been prepared based on Co,[4−8] Ir,[9−11] and Fe,[12] though some concerns about stability were raised.[13,14] Di-Ru[15−17] and mono-Ru[18−23] complexes are well established homogeneous catalysts for water splitting. Chemical ligation affects the redox properties and catalytic reactivity of these complexes, but no structure−activity relationships are currently known; therefore, researchers have to develop these systems by a trial-and-error approach. The majority of single-site Ru catalysts utilize neutral polypyridine based ligands and water as the only oxygen containing ligand.[18−24] Some di-Ru catalysts might have additional oxygen ligands due to bridging oxygen (e.g., blue dimer)[15] or quinone[16] coordinated to Ru. Single-site Ru catalysts with mixed nitrogen and oxygen ligation are also active.[1,25]

Until recently, mechanistic analysis with spectroscopic identification of reactive intermediates was only available for a blue dimer (BD) and suggested formation of highly oxidized Ru^{V},Ru^{V} and Ru^{IV},Ru^{V} species as catalytically important intermediates.[26,27] Formation of BD in the Ru^{IV},Ru^{V} oxidation state was later confirmed,[28] and the spin density of the radicaloid Ru^{V}=O fragment was mapped experimentally.[29] Spectroscopic signatures attributed earlier to Ru^{V},Ru^{V} state of BD (including an $S = 1/2$ EPR signal) were later re-evaluated.[30]

Received: January 10, 2014
Revised: June 30, 2014
Published: August 5, 2014

   dx.doi.org/10.1021/ja506586b | J. Am. Chem. Soc. 2014, 136, 11938−11945

For newly developed single-site Ru catalysts, it has been widely postulated (without direct experimental proof) that a Ru^{V}=O intermediate is a kinetically resolved species which reacts with water slowly.[19,31−37] Reported rate constants for Ru^{V}=O formation and its reaction with water imply the catalytic steady state is composed of the Ru^{V}=O form of the catalyst.[31,32,38] A reaction pathway via Ru^{IV} was determined for one catalyst at neutral and basic conditions, while the Ru^{V} pathway was implied at acidic pH.[24] See Figure 1 for a summary of proposed pathways.

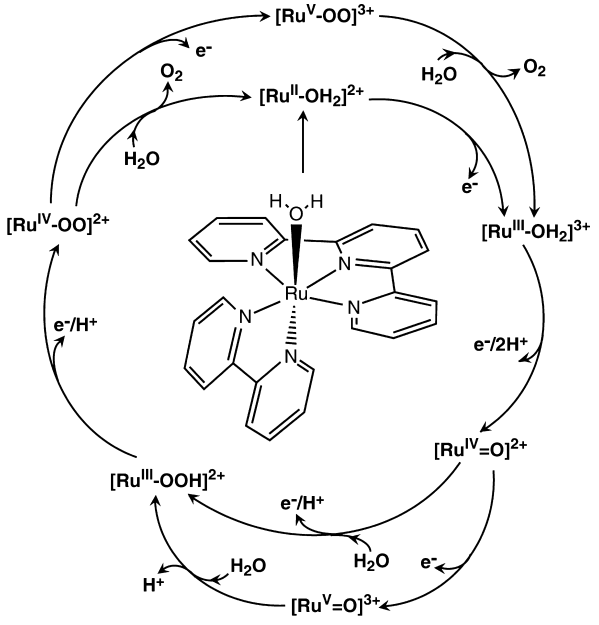

Figure 1. Proposed mechanism for water oxidation catalyst $[Ru^{II}(bpy)(tpy)H_2O]^{2+}$.

To gain spectroscopic information about the catalytic mechanism, we analyzed a water oxidation catalyst $[Ru^{II}(bpy)(tpy)H_2O]^{2+}$ (bpy = 2,2′-bipyridine, tpy = 2,2′;6′,2″-terpyridine) representative of the class of polypyridine based single-site Ru catalysts using electron paramagnetic resonance (EPR) and X-ray spectroscopy. Among the Ru polypyridine catalysts for water oxidation,[12,17−19,21−23,32,39,40] $[Ru^{II}(bpy)(tpy)H_2O]^{2+}$ is by far the most studied single-site catalyst.[19,20,22,31,33,36,38,41,42] It has an interesting history of having been thoroughly studied in the past without notice of its catalytic activity in water oxidation.[43] Recently, it was a source of controversy regarding catalytic activity of its halogenated derivatives,[20,36,44] including $[Ru^{II}(bpy)(tpy)Cl]^{+}$ which we also studied here in parallel with $[Ru^{II}(bpy)(tpy)H_2O]^{2+}$. According to the current water oxidation paradigm, $[Ru^{II}(bpy)(tpy)Cl]^{+}$ should not work as a water oxidation catalyst as it lacks the Ru−H_2O fragment which can undergo proton coupled electron transfer (PCET) and formation of an activated Ru=O species. Our spectroscopic and computational analysis clarified mechanistic aspects of water activation in representative $[Ru^{II}(bpy)(tpy)H_2O]^{2+}$ catalyst.

2. MATERIALS AND METHODS

2.1. Sample Preparation. Throughout this study the $[Ru^{II}(bpy)(tpy)Cl]^{+}$ (bpy = 2,2′-bipyridine, tpy = 2,2′;6′,2″-terpyridine) complex was used as a Cl^{-} salt.[20] Note that all experiments with $[Ru^{II}(bpy)(tpy)Cl]Cl$ salt dissolved in water should be performed immediately (within 2 min) to avoid onset of Ru−Cl exchange. For optimal experimentation, the $[Ru^{II}(bpy)(tpy)Cl]Cl$ solution was aliquoted into small plastic tubes and frozen for further use. $[Ru^{II}(bpy)(tpy)H_2O](PF_6)_2$ was used as a reference compound. Incubation of $[Ru^{II}(bpy)(tpy)Cl]Cl$ in water for 24 h resulted in $[Ru^{II}(bpy)(tpy)H_2O]Cl_2$. Ultrapure (Type 1) water (resistivity 18.2 MΩ cm at 25 °C, TOC 4 μg/L) was used for solutions. All samples were prepared in 0.1 M HNO_3 acid, pH 1.0 (catalog no. 225711 from Sigma-Aldrich). Oxidant solutions were prepared fresh daily by dissolving $Ce(NH_4)_2(NO_3)_6\cdot 4H_2O$ in 0.1 M HNO_3. A Cary 300 Bio UV−vis spectrophotometer (Varian, Inc.) was used to monitor UV−visible spectra (5×10^{-5} M concentration). Solutions for preparation of EPR samples were bubbled with argon to displace dissolved oxygen.

2.2. Oxygen (O_2) Evolution Measurements. Oxygen evolution was measured with a PC operated Clark type polarographic oxygen electrode from Oxygraph System (Hansatech Instruments Ltd.). The sample was housed within a hermetic borosilicate glass reaction vessel, thus preventing penetration of any atmospheric oxygen. Calibration was carried out by measurements of the signal from O_2-saturated water in an open reaction vessel. Sodium dithionite, an oxygen depleting agent, was added to the water, and the drop in the signal was related to the solubility of oxygen in water at room temperature (262 μmol/L). The glass vessel was thoroughly washed with water and 1 mL of 0.65 mM $[Ru^{II}(bpy)(tpy)Cl]Cl$ solution in water was added. A defined number of Ce^{IV} equivalents (usually 20 equiv in 1 M HNO_3) were carefully added by means of a Hamilton syringe into the chamber through a plunger screw, and oxygen evolution was measured as a function of time. Dilution of Ce^{IV} solution was adjusted to 10:1 to allow for final pH = 1.

2.3. EPR Measurements. Low-temperature X-band EPR spectra were recorded by using a Bruker EMX X-band spectrometer equipped with an X-Band CW microwave bridge. The sample temperature was maintained at 20 K, unless otherwise indicated, by use of an Air Products LTR liquid helium cryostat. Spectrometer conditions were as follows: microwave frequency, 9.65 GHz; field modulation amplitude, 10 G at 100 kHz; microwave power, 31.70 mW. Standard EPR sample tubes were filled with sample through all of the resonator space, a septum was placed on top, and sample space was evacuated to prevent oxygen condensation. Whenever relative signal intensities are discussed, measurements were conducted on the same day in the same conditions to allow direct comparison of the signal intensities. Field calibration was checked versus a DPPH standard.

2.4. Ru L-Edges X-ray Absorption Near-Edge Spectroscopy (XANES) Measurements. Ru $L_{2,3}$ XANES spectra were collected at the Advanced Photon Source (APS) at Argonne National Laboratory on beamline 9-BM at a photon energy of 2.3−3.0 keV and an average current of 100 mA. A Si(111) crystal monochromator with approximately 0.3 eV energy resolution was used, and the intensity of the incident X-rays was monitored by an ion chamber (I_0) in front of the sample. Data on solutions were recorded as fluorescence excitation spectra using a Si 4-element energy-resolving detector. The solution samples were kept at 80 K using a Linkam cryostage in a He atmosphere at ambient pressure. To reduce X-ray induced sample damage, 80% flux was used; no damage was observed in consecutive scans. No more than three scans were taken at each sample position. Energy was calibrated with S K-edge of sodium thiosulfate at 2469.20 eV. The edge position was determined by the inflection point evaluated as a second derivative zero-crossing. Spectra were normalized by fitting the 150 eV range above the Ru L_3-edge with a third-order polynomial.

2.5. Ru K-Edge X-ray Absorption Spectroscopy (XAS) Measurements. Ru K-edge XAS spectra were collected at the Advanced Photon Source (APS) at Argonne National Laboratory on BM-20 beamline at incident photon energy 23 keV and an average current of 100 mA. The radiation was monochromatized by a Si(110) crystal monochromator. The intensity of the X-rays was monitored by three ion chambers (I_0, I_1, and I_2) filled with 70% nitrogen and 30% argon and placed before the sample (I_0) and after the sample (I_1 and I_2). Ru metal was placed between the I_1 and I_2, and its absorption was recorded with each scan for energy calibration. Plastic (Lexan) EXAFS sample holders (inner dimensions of 12 mm × 3 mm × 3 mm) filled with frozen solutions were inserted into precooled (20 K) cryostat. The samples were kept at 20 K in a He atmosphere at ambient pressure. Data were recorded as fluorescence excitation spectra using a Ge 13-element energy-resolving detector. Solid samples were diluted with BN powder

dx.doi.org/10.1021/ja506586b | J. Am. Chem. Soc. 2014, 136, 11938−11945

in a 1:5 ratio, pressed between mylar tape, and measured in the cryostat in transmission mode. To reduce the risk of sample damage by X-ray radiation, 80% flux was used in the defocused mode (beam size 1 × 8 mm) and no damage was observed in multiple scans. The samples were also protected from the X-ray beam during motor movements by a shutter synchronized with the scan program. Additionally, low flux measurements (only 10% of beamline flux) were done on reactive intermediates to demonstrate the same EXAFS results. No more than 5 scans were taken at each sample position at any condition.

Ru XAS energy was calibrated by the first maxima in the derivative of the ruthenium metal XANES spectrum (22117 eV). EXAFS data were collected during a total of three beamtimes. EXAFS scan with 10 eV steps in the pre-edge region (21 967−22 102 eV), 1 eV steps (22 102−22 117 eV) through the edge and 0.05 $Å^{-1}$ steps from k = 2.0−16 $Å^{-1}$ were used. As reference compounds for high Ru oxidation states, Ru^{IV} and Ru^{V}, Ru^{IV} oxide, and tetra-*n*-propylammonium bis-2-hydroxy-2-ethylbutyrato(oxo) ruthenate(V)[45] were used.

2.6. Density Functional Theory (DFT) Calculations. DFT calculations were performed with Gaussian09[46] using the CPCM polarizable conductor model for water solvation. Two explicit water molecules were included for precursor catalysts and one explicit water molecule remained in reactive intermediates with the O−O bond. The B3LYP exchange-correlation (XC) functional was used. The 6-31G* basis set was used for all organic atoms (C, O, N, H). The DGDZVP basis set with all electrons of the Ru atom explicitly included in calculations (no frozen cores) as well as the frozen core LANL2DZ were used for Ru. Geometry optimizations and ΔG calculations were performed, Tables 1 and 3, and Supporting Information Tables S1−S3. Unless otherwise noted, results of UB3LYP with DGDZVP (Ru) and 6-31G* (light elements) were presented through the text.

DFT calculations were also performed with the Amsterdam Density Functional (ADF)[47] 2012 package to optimize geometry and predict the *g*-tensor in EPR. The local density approximation (LDA) XC functional with polarized triple-ζ Slater-type orbital basis set (TZ2P) was used without the frozen core approximation. Relativistic effects were accounted for by simulations within the spin−orbit zeroth-order regular approximation (ZORA) Hamiltonian. ADF calculations were performed for systems in gas phase.

3. RESULTS

3.1. EPR Analysis of Paramagnetic S = 1/2 Intermediates. EPR is uniquely sensitive to paramagnetic intermediates: Ru^{III} (d^5) and Ru^{V} (d^3) complexes. Ru^{IV} complexes are EPR silent. Figure 2A shows the formation of paramagnetic $[Ru^{III}(bpy)(tpy)H_2O]^{3+}$ complex with g_{xx} = 2.60, g_{yy} = 2.40, and g_{zz} = 1.66 upon addition of 1 equiv of Ce(IV) in 0.1 M HNO_3. Its *g*-tensor is within the typical range for Ru^{III} complexes with nitrogen and oxygen ligands.[48] Figure 2A shows that upon addition of excess (20 equiv) of Ce^{IV} and freezing within 30 s after mixing, $[Ru^{II}(bpy)(tpy)H_2O]^{2+}$ undergoes further oxidation to EPR silent form. The intensity of the remaining EPR signal is less than 5%, note that mixing was done to ensure identical final concentration of Ru complex in both samples. Figure 2B shows the residual EPR signal (less than 5%, see Figure 2A for relative comparison) for catalytic mixtures in H_2O and D_2O (pH = 1) prepared and frozen within 30 s. EPR signals in Figure 2B were collected with higher gain and improved statistics. The EPR spectra in H_2O and D_2O solutions, Figure 2B, are similar. They contain unique EPR signal with g_{xx} = 2.31, g_{yy} = 2.20, and g_{zz} = 1.91 likely representing a Ru^{III} complex with a significantly modified ligand environment. Other spectral components at g = 2.76, and g = 2.46 are due to remaining $[Ru^{III}(bpy)(tpy)H_2O]^{3+}$ and/or a small mixture of $[Ru^{III}(bpy)(tpy)Cl]^{2+}$ which served as a precursor in the synthesis. Supporting Information Figure S3 shows EPR results for $[Ru^{III}(bpy)(tpy)Cl]^{2+}$. The unique g_{xx} = 2.31, g_{yy} = 2.20, g_{zz} = 1.91 signal can correspond to spin S = 1/2 peroxo intermediates $[Ru^{III}(bpy)(tpy)OOH]^{2+}$ or $[Ru^{III}(bpy)(tpy)OO]^{+}$. Interestingly, both EPR spectra, Figure 2B, lack evidence of $[Ru^{V}(bpy)(tpy)=O]^{3+}$ intermediate. Ru^{V}=O species have a very characteristic *g*-tensor which is more isotropic in comparison with Ru^{III} and has all three components close to g = 2 and Ru (I = 5/2) hyperfine splittings.[49,50] Freeze quench at different times did not reveal EPR signatures of $[Ru^{V}(bpy)(tpy)=O]^{3+}$ intermediate, Supporting Information Figure S2.

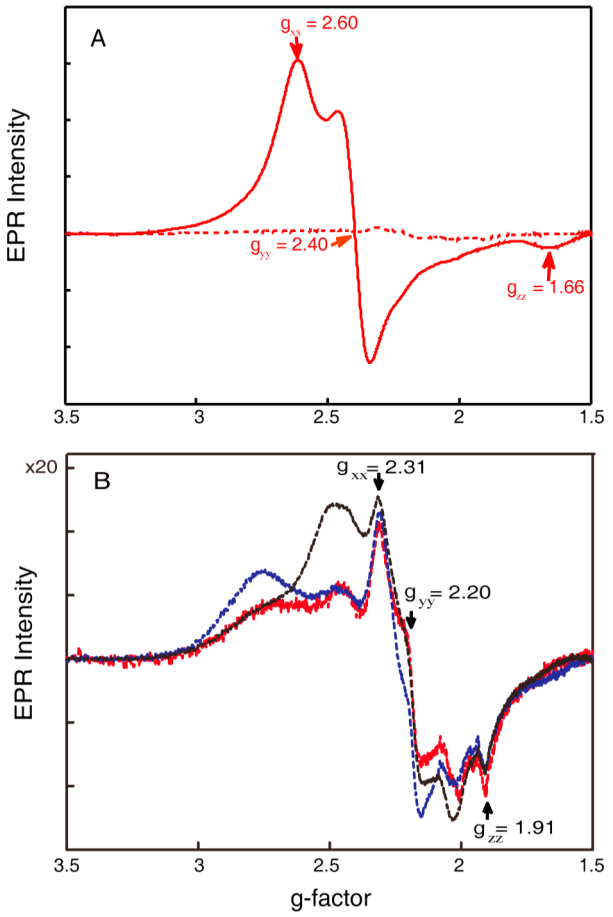

Figure 2. X-Band EPR (20 K) of 1 mM solutions of (A) $[Ru^{III}(bpy)(tpy)H_2O]^{3+}$ (red) and catalytic mixture (red dash) generated by adding 20 equiv of Ce^{IV} to $[Ru^{II}(bpy)(tpy)H_2O]^{2+}$ in 0.1 M HNO_3. (B) Zoom (×20) into low intensity EPR signals from solutions generated by adding 20 equiv of Ce^{IV} in 0.1 M HNO_3 to $[Ru^{II}(bpy)(tpy)H_2O]^{2+}/H_2O$ (red) and to $[Ru^{II}(bpy)(tpy)D_2O]^{2+}/D_2O$ (blue), compared to solution generated by adding 100 mM Ce^{IV} to $[Ru^{II}(bpy)(tpy)H_2O]^{2+}/H_2O$ (black) in 1 M HNO_3 (pH = 0). All samples were frozen within 30 s.

3.2. Chemical Composition of the Catalytic Steady State. Ru L- and K-edges XANES spectra were used to assess the Ru oxidation state in prepared mixtures, Figure 3. Spectra of $[Ru^{II}(bpy)(tpy)H_2O]^{2+}$ oxidized with 20 equiv of Ce^{IV} show a significant shift to higher energy consistent with formation of Ru^{IV}. However, the edge position of the oxidized $[Ru^{II}(bpy)(tpy)Cl]^{+}$ sample is more consistent with the presence of $[Ru^{III}(bpy)(tpy)Cl]^{2+}$. XANES data are in agreement with EPR results (Supporting Information Figure S3) and show that retention of the Ru−Cl bond impedes oxidation past the Ru^{III} state due to inaccessibility of PCET. Note that the Ru K-edge shift to higher energy recorded here for Ru^{IV} versus Ru^{III} is larger than shown in Vigara et al.[37] for oxidation of $[Ru^{II}(damp)$-

dx.doi.org/10.1021/ja506586b | J. Am. Chem. Soc. 2014, 136, 11938−11945

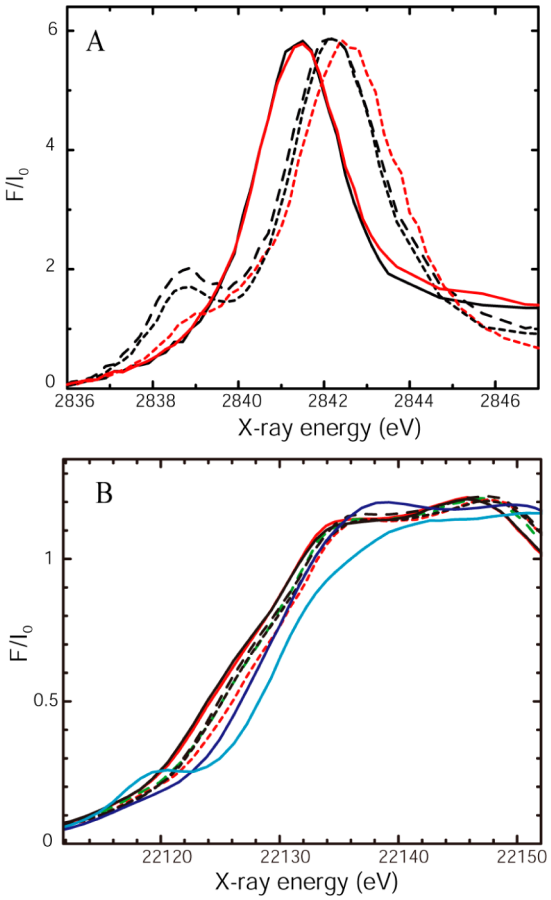

Figure 3. Normalized Ru L_3-edge (A) and Ru K-edge XANES (B) of the starting $[Ru^{II}(bpy)(tpy)Cl]^+$ (black) and $[Ru^{II}(bpy)(tpy)H_2O]^{2+}$ (red) complexes; $[Ru^{II}(bpy)(tpy)Cl]^+$ complex oxidized with 1 equiv (black long dashed line) and 20 equiv (black dashed line) of Ce^{IV} and $[Ru^{II}(bpy)(tpy)H_2O]^{2+}$ oxidized with 20 equiv of Ce^{IV} (red dashed line). Catalyst concentration is 1 mM in 0.1 M HNO_3. Panels B also shows comparison with $[Ru^{II}(bpy)(tpy)H_2O]^{2+}$ oxidized with 1 equiv of Ce^{IV} (green dashed line), RuO_2 (blue), and tetra-*n*-propylammonium bis-2-hydroxy-2-ethylbutyrato(oxo) ruthenate(V)[45] reference compounds (light blue).

$(bpy)H_2O]^{2+}$. This is likely due to a more complete (95% by EPR) conversion to Ru^{IV} state achieved in our experiment. Ru K-edge XANES measured from samples actively evolving oxygen at longer (up to 4 h, see Figure 4 for EXAFS) times shown same edge position and are not plotted.

Two rate-limiting steps were reported for water oxidation with $[Ru^{II}(bpy)(tpy)H_2O]^{2+}$:[33] $Ru^V{=}O$ reaction with H_2O or O_2 release from $Ru^{IV}OO$ intermediate. The EPR analysis rules out the former but might still be consistent with later. Thus, analysis of the ligand environment of Ru^{IV} is critical to confirm or eliminate the latter rate-limiting step. Figure 4 compares EXAFS data for $[Ru^{II}(bpy)(tpy)H_2O]^{2+}$ and catalytic mixture prepared by adding 20 equiv of Ce^{IV}. EXAFS fitting (Table 1, Supporting Information Figure S4) shows the Ru=O distance at 1.82 Å which is consistent with assignment as a $[Ru^{IV}(bpy)(tpy){=}O]^{2+}$ intermediate. The detected 1.8 Å distance is not compatible with a $Ru^{IV}OO$ intermediate. For $[Ru^{IV}OO]^{2+}$ complex, DFT predicted a Ru−O distance of 2.08 Å, Supporting Information Table S1. $Ru^V{=}O$ should have shorter Ru−O distance (about 1.7 Å[28]); thus, EXAFS and XANES results provide additional reassurance of the absence of a $Ru^V{=}O$ intermediate. Note that

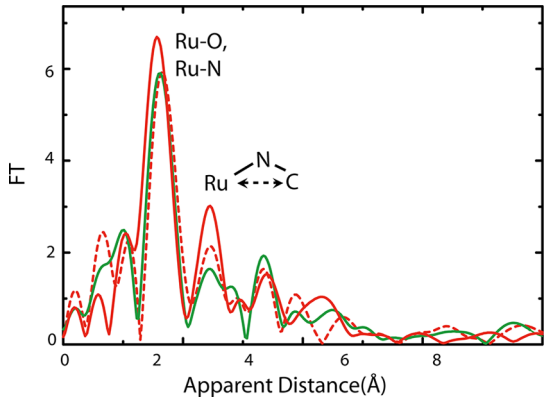

Figure 4. Ru K-edge EXAFS of the starting $[Ru^{II}(bpy)(tpy)H_2O]^{2+}$ (red); $[Ru^{IV}(bpy)(tpy){=}O]^{2+}$ prepared by oxidation of $[Ru^{II}(bpy)(tpy)H_2O]^{2+}$ with 20 equiv of Ce^{IV} and frozen in 30 s (dash red) and catalytic mixture of $[Ru^{II}(bpy)(tpy)H_2O]^{2+}$ with 330 equiv of Ce^{IV} frozen after 4 h (green). Catalyst concentration is 1 mM in 0.1 M HNO_3.

Table 1. Parameters of EXAFS Fits

fit	shell, N^a	R, Å	σ^2 (10^{-3})	R-factor	reduced χ-square
		$[Ru^{II}(bpy)(tpy)H_2O]^{2+}$			
1	Ru−N, 6	2.07	5.3	0.30	681
2[b]	Ru−N, 6	2.06	5.2	0.13	383
	Ru−C, 10	2.99	10.9		
		$[Ru^{IV}(bpy)(tpy){=}O]^{2+,c}$			
3	Ru−N, 6	2.09	5.2	0.27	52
4	Ru−N, 6	2.09	4.8	0.14	41
	Ru−C, 10	2.50	17.8		
5	Ru−O, 1	1.79	1.2	0.07	36
	Ru−N, 5	2.10	4.9		
	Ru−C, 10	3.08	15.0		
6	Ru−O, 1	1.82	1.5	0.05	46
	Ru−N, 5	2.06	2.7		
	Ru−C, 6	2.90	2.2		
	Ru−C, 4	3.06	2.2		
$[Ru^{II}(bpy)(tpy)H_2O]^{2+}$ + 330 equiv Ce^{IV} after 4 h of O_2 evolutions, peak I					
7	Ru−N, 6	2.08	5.1	0.049	12575
8	Ru−O, 1	1.79	2.6	0.0001	49.8
	Ru−N, 5	2.08	4.1		
		$[Ru^{II}(bpy)(tpy)Cl]^{+,d}$			
9	Ru−N, 6	2.03	5.2	0.57	9141
10	Ru−N, 6	2.02	5.0	0.40	8904
	Ru−C, 10	2.89	7.1		
11	Ru−N, 5	2.01	4.3	0.09	3252
	Ru−Cl, 1	2.41	1.9		
	Ru−C, 10	2.88	6.1		
		$[Ru^{III}(bpy)(tpy)Cl]^{2+,e}$			
12	Ru−N, 6	2.07	5.2	0.39	6497
13	Ru−N, 6	2.07	5.1	0.30	7217
	Ru−C, 10	2.99	10.6		
14	Ru−N, 5	2.07	3.4	0.11	3300
	Ru−Cl, 1	2.34	3.5		
	Ru−C, 10	3.01	11.3		

[a] N, number of vectors is given per Ru center; S_0^2 = 1 was fixed. [b] Further increase in number of shells did not result in better fits. [c] $Ru^{IV}{=}O$ from DFT 1.81 Å. [d] Ru−Cl from XRD 2.40 Å,[51] from DFT 2.43 Å. [e] Ru−Cl from DFT 2.33 Å.

X-ray induced damage to $Ru^V{=}O$ intermediate has been excluded. Ru^{IV},Ru^V intermediate was not susceptible to any detectable X-ray modifications after prolonged exposures in same

dx.doi.org/10.1021/ja506586b | J. Am. Chem. Soc. 2014, 136, 11938−11945

experimental conditions[28] (note use of bending magnet beamline, defocused beam and 20 K temperature).

We decided to use EXAFS to monitor catalyst structural integrity under prolonged catalytic activity. Figure 4 shows EXAFS recorded after 4 h of O_2 evolution with addition of 330 equiv of Ce^{IV}. The first coordination sphere of Ru was determined to be largely unchanged with Ru=O at 1.79 Å and Ru−N at 2.08 Å, Table 1. Ru−C peak at 3.00 Å decreased in intensity likely due to increased heterogeneity. We conclude that the Ru^{IV}=O moiety persists in catalytic solution under prolonged O_2 evolution. EPR spectra of this sample represented very broad, unstructured signal due to large content of dissolved O_2 (data not shown). EXAFS shown no formation of dimer species which is also in agreement with earlier mass spec results.[31] EXAFS analysis of $[Ru^{II}(bpy)(tpy)Cl]^+$ oxidized with excess of Ce^{IV} shows retention of the Ru−Cl bond (Supporting Information Figure S5, Table 1). Oxidation results in the shortening of the Ru−Cl bond from 2.41 Å in the Ru^{II} complex to 2.34 Å in the Ru^{III} complex.

To make a final clarification to a debate about possible catalytic activity of $[Ru^{II}(bpy)(tpy)Cl]^+$, spectroscopic observations were paralleled with catalytic measurements. O_2 evolution was measured from reaction mixtures prepared by incubating $[Ru^{II}(bpy)(tpy)Cl]^+$ in water for 2 min, 30 min, and 4 h and adding 20 equiv of Ce^{IV}. We found that $[Ru^{III}(bpy)(tpy)Cl]^{2+}$ formed upon Ce^{IV} addition is not a catalyst for water oxidation and it does not gain catalytic activity upon prolonged (5000 s) incubation with 20 equiv of Ce^{IV}, Figure 5. Thus, the exchange of Cl^- ligand to H_2O is required to form the active catalyst.

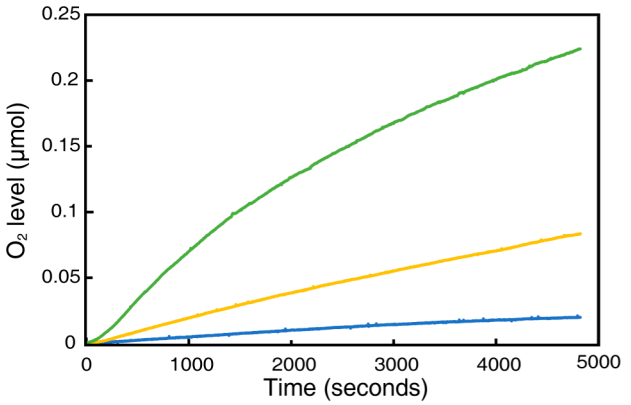

Figure 5. Kinetics of O_2 evolution recorded with oxygen electrode. $[Ru^{II}(bpy)(tpy)Cl]^+$ was incubated in water for 2 min (blue), 30 min (orange), and 4 h (green) and 20 equiv of Ce^{IV} was added to initiate catalysis. Conditions: 0.1 M HNO_3, room temperature.

3.3. DFT Analysis. Molecular geometries derived by DFT optimization (Table 1 and Supporting Information Tables S1 and S3) are in good agreement (within the error of ±0.02 Å) with XRD (Ru−Cl distance)[51] and EXAFS (Ru−Cl and Ru^{IV}=O distances) results. Using a full electron basis set as compared to the 28 electron frozen core basis made very little difference in molecular geometry, see Supporting Information Table S1 for comparison.

We encountered a new EPR signal in our experiment and proposed that it originates from a Ru complex with a significantly modified ligand environment. To investigate this proposal, we compared experimental and relativistic DFT (ADF) computed *g*-tensors for complexes in this study (Table 2). We found that DFT reproduces g_{xx} and g_{yy} components of known EPR signals

Table 2. Summary of *g*-Tensor Parameters from Experiment and DFT (ADF) Calculations

		g_{xx}	g_{yy}	g_{zz}
$[Ru^{III}(bpy)(tpy)Cl]^{2+}$	experiment	2.79	2.25	1.66
	DFT	2.69	2.16	1.94
	difference	0.10	0.09	0.28
$[Ru^{III}(bpy)(tpy)H_2O]^{3+}$	experiment	2.60	2.40	1.66
	DFT	2.47	2.34	1.89
	difference	0.13	0.06	0.23
unknown intermediate	experiment	2.31	2.20	1.91
$[Ru^{III}(bpy)(tpy)OOH]^{2+}$	DFT	2.15	2.09	1.98
	difference	0.16	0.11	0.07
$[Ru^{III}(bpy)(tpy)OO]^+$	DFT	2.08	2.03	2.00
	difference	0.23	0.17	0.09

within 0.1; however, a larger error up to 0.28 was found for g_{zz} component. DFT predicts that both the Ru-OOH and deprotonated RuOO complexes will have significantly upfield shifted g_{xx} and g_{yy} components in comparison with the Ru^{III}−H_2O complex. Thus, assignment of $[Ru^{III}(bpy)(tpy)OOH]^{2+}$ peroxide is plausible but hard to confirm due to very low concentration of the species (less than 5%). Other catalysts will be similarly analyzed to search for a system affording a larger steady-state concentration of peroxide.

DFT was performed to calculate the ΔG^0 of elemental steps in catalytic reaction of $[Ru^{II}(bpy)(tpy)H_2O]^{2+}$, Table 3 and Supporting Information Table S1, with two and one explicit water molecules and CPCM water solvation. Taking the value of the reference potential (NHE) of 4.44 V and the solvation free energy of a proton of −11.64 V as in[35] (Supporting Information Table S1), the redox potential E^0 for the series of catalytic steps was computed, Supporting Information Table S1, Table 3, and Figure 6. ΔG^0 values were obtained for basis sets with all Ru electrons (DGDZVP) and frozen core (LANL2DZ) see Supporting Information Table S1 for comparison; in the text we refer to numbers obtained using DGDZVP.

A redox potential of 2.13 V computed for $[Ru^{IV}(bpy)(tpy)$=$O]^{2+}$/$[Ru^{V}(bpy)(tpy)$=$O]^{3+}$ is in agreement with the other reported theoretical value of 2.21 V[35] and is out of reach of Ce^{IV} oxidant solution (1.47 V[31,38] in 0.1 M HNO_3). To additionally verify performance of DFT for prediction of redox potentials for highly oxidized Ru^V and Ru^{VI} species, we computed redox potentials for consecutive oxidation of $[Ru^{II}(bpy)_2(H_2O)_2]^{2+}$ catalysts, Table 3 and Supporting Information Table S2. For $[Ru^{II}(bpy)_2(H_2O)_2]^{2+}$ catalysts, redox potentials for all steps are available from literature,[52] Table 3, and formation of Ru^V intermediate was verified by EPR.[53] Table 3 illustrates that for $[Ru^{II}(bpy)_2(H_2O)_2]^{2+}$ catalysts, the maximum deviation between DFT derived and experimental redox potentials is 0.16 V. Same is true for 1 and 2 electron oxidation of $[Ru^{II}(bpy)(tpy)$-$H_2O]^{2+}$. Deviation up to 0.5 V between DFT derived and reported[33] $[Ru^{IV}(bpy)(tpy)$=$O]^{2+}$/$[Ru^{V}(bpy)(tpy)$=$O]^{3+}$ redox couple (Table 3) significantly exceeds the error expected for DFT. This is in good agreement with absence of $[Ru^{V}(bpy)(tpy)$=$O]^{3+}$ spectroscopic signatures.

4. DISCUSSION

In this paper, we report EPR and X-ray spectroscopic characterization of the electronic structure and molecular geometry of the $[Ru^{II}(bpy)(tpy)H_2O]^{2+}$ and $[Ru^{II}(bpy)(tpy)$-$Cl]^+$ complexes and their respective intermediates of catalytic water oxidation. As our results show, $[Ru^{II}(bpy)(tpy)Cl]^+$ is not

dx.doi.org/10.1021/ja506586b | J. Am. Chem. Soc. 2014, 136, 11938−11945

Table 3. Comparison of DFT (UB3LYP/DGDZVP) Estimated and Experimentally Reported Redox Potentials (E^0)

elemental steps	DFT E^0/V	experiment E^0/V	difference (experiment − DFT)
	$[Ru^{II}(bpy)(tpy)H_2O]^{2+}$		
$Ru^{III}–H_2O + 1e^- = Ru^{II}–H_2O$	1.06	1.04[43]	−0.02
$Ru^{IV}=O + 1e^- + 2H^+ = Ru^{III}–H_2O$	1.23	1.39[43]	+0.16
$Ru^{V}=O + 1e^- = Ru^{IV}=O$	2.13	1.60;[33] 1.73;[54] 1.80[38]	−0.53; −0.40; −0.33
	$[Ru^{II}(bpy)_2(H_2O)_2]^{2+}$		
$Ru^{III}–(H_2O)_2 + 1e^- = Ru^{II}–(H_2O)_2$	1.04	0.88[52]	−0.16
$Ru^{IV}–(OH)_2 + 1e^- + 2H^+ = Ru^{III}–(H_2O)_2$	1.18	1.19	+0.01
$Ru^{V}=O,–OH + 1e^- + 1H^+ = Ru^{IV}–(OH)_2$	1.47	1.34	−0.13
$Ru^{VI}(=O)_2 + 1e^- + 1H^+ = Ru^{V}=O,–OH$	1.54	1.50	+0.04

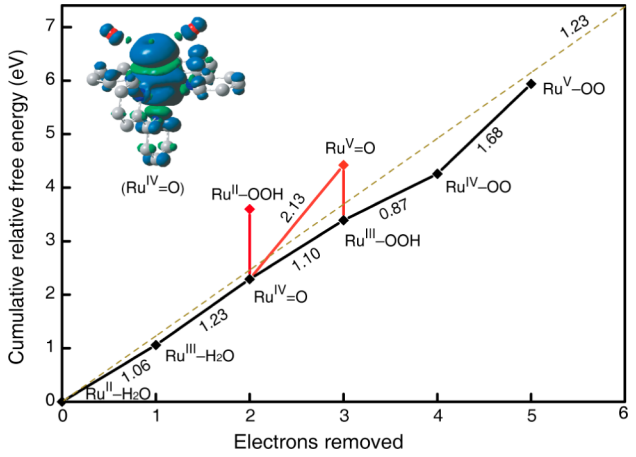

Figure 6. DFT (UB3LYP/DGDZVP) derived Latimer−Frost diagram for oxidation of $[Ru^{II}(bpy)(tpy)H_2O]^{2+}$ under standard conditions (pH = 0). Main path (black diamonds) and paths with significant barriers (red diamonds). Dashed line shows 1.23 eV water oxidation potential at pH = 0. Inset: the spin density of $Ru^{IV}=O$ species.

an active catalyst but a precursor to the $[Ru^{II}(bpy)(tpy)H_2O]^{2+}$ complex which is capable of water oxidation. Combined EPR, XANES, and EXAFS show that catalytic steady state of $[Ru^{II}(bpy)(tpy)H_2O]^{2+}$ contains ∼95% $[Ru^{IV}(bpy)(tpy)=O]^{2+}$. The remaining ∼5% might correspond to the peroxo species.

Understanding catalytic water oxidation requires identification of the species involved in the formation of the O−O bond. It has been widely postulated (without direct experimental proof) that the $Ru^{V}=O$ intermediate is an active species required for water activation in single-site Ru catalysts and its reactivity with water represents a rate-limiting step.[19,31−37] It is productive at this point to review both the electrochemical and UV−vis kinetic evidence which are currently used in support of a $Ru^{V}=O$ intermediate.

We start with review of electrochemical evidence of Ru^{V} formation. Table 3 summarizes the different values of redox potential that were reported for Ru^{IV}/Ru^{V} couple. During the first detailed investigation, this particular redox couple and the overall catalytic activity of $[Ru^{II}(bpy)(tpy)H_2O]^{2+}$ escaped detection.[43] In 2008 the Meyer group reassured "that there is no evidence for further (beyond Ru^{IV}) oxidation of this complex to the solvent limit at ∼1.8 V, and it is not a catalyst for water oxidation".[19] The first report on the catalytic activity of $[Ru^{II}(bpy)(tpy)H_2O]^{2+}$ in water oxidation was in 2009 by Masaoka and Sakai.[36] In 2010 the Meyer group also reported that $[Ru^{II}(bpy)(tpy)H_2O]^{2+}$ is an active water oxidation catalyst.[33] The redox potential of the Ru^{IV}/Ru^{V} couple was given as 1.6 V,[33] but no explanation of the discrepancy with the earlier 1984 and 2008 reports was provided. It is clear from the above discussion and additional recent studies[41,42] that there has been historically significant uncertainty in determining this redox potential.

DFT calculations aimed at reproducing the proposed mechanism of water splitting with $Ru^{V}=O$ as a key catalytic intermediate also consistently report extreme inconsistencies (well above the typical (∼200 mV) DFT uncertainty) for the redox potential of the Ru^{IV}/Ru^{V} couple. For instance, E^0 was computed to be 2.13 V here (Table 3) and 2.21 V in Hughes et al.,[35] and 1.98 V[34] was reported for a very similar $[Ru^{II}(bpm)(tpy)H_2O]^{2+}$ catalyst. Summarizing the above information, we note that reliable electrochemical separation of $[Ru^{IV}(bpy)(tpy)=O]^{2+}/[Ru^{V}(bpy)(tpy)=O]^{3+}$ oxidation from the catalytic wave of water oxidation remains uncertain and may even prove impossible. No *in situ* spectroscopy was performed at 1.6−1.8 V applied potential for this or any other similar complex to verify the presence of $[Ru^{V}(bpy)(tpy)=O]^{3+}$. Such verification is a complex study outside the scope of this manuscript. The large discrepancy between DFT and experimental reports for the Ru^{IV}/Ru^{V} couple as well as inconsistencies between experimental reports indicate the inconclusive assignment of the observed electrochemical process. The nature of this process should be further investigated in the future for a better understanding of electrochemical water oxidation catalysis.

We continue with a review of O_2 evolution under chemical oxidation. O_2 evolution kinetics by $[Ru^{II}(bpy)(tpy)H_2O]^{2+}$ were reported to be first order in the Ru catalyst and zeroth order in Ce^{IV}[31,33,54] This is consistent with either rate-limiting $Ru^{V}=O$ reactivity toward water (k_{O-O}), or rate-limiting O_2 loss from the $Ru^{IV}(OO)$ intermediate, k_4. However, a different kinetic law with catalytic O_2 evolution being first order in the Ru catalyst as well as first order in Ce^{IV} was reported by Masaoka and Sakai.[36]

The manuscript by Yagi et al.[22] clarifies the discrepancy by reporting that the rate law changes depending on the oxidant concentration. The following rate constants were reported in 0.1 M HNO_3: $k_3 = 4\ M^{-1}\ s^{-1}$[38] ($Ru^{IV}=O$ to $Ru^{V}=O$ oxidation) and $k_{O-O} = 2.3 \times 10^{-4}\ s^{-1}$ in ref 38 and $1.9 \times 10^{-4}\ s^{-1}$ in ref 33 (oxygen−oxygen bond formation or k_4). These imply a significant (up to 100% of Ru species) buildup of the $Ru^{V}=O$ intermediate in solutions on the seconds time scale. However, no independent spectroscopic evidence confirming the presence of $Ru^{V}=O$ species was given in either study. In contrast, the ESI-MS results were consistent with the absence of a $Ru^{V}=O$ intermediate.[31] The Berlinguette group first pointed out the large discrepancy in the redox potential of the Ru^{IV}/Ru^{V} couple and the driving force available from the Ce^{IV} oxidant (about 1.45 V in 0.1 M HNO_3),[31,38] (all redox potentials are given relative to NHE). Using the Ce^{III}/Ce^{IV} (1.45 V) and Ru^{IV}/Ru^{V} (1.80 V)[38] one can derive the ratio of Ru^{V} to Ru^{IV} to be on the order of 10^{-6}

dx.doi.org/10.1021/ja506586b | J. Am. Chem. Soc. 2014, 136, 11938−11945

which critically contradicts the results of kinetic modeling. Thus, one set of reported numbers (either rate constants or redox potentials) must be incorrect. It is possible that the rate constant for Ru^{V}=O formation (k_3 = 4 M^{-1} s^{-1}) is incorrect as is it based on indirect (i.e., insensitive to electronic structure) UV−vis measurements.

Here, we did a careful investigation to determine whether any Ru^{V}=O species could be detected in the reaction mixtures under catalytic conditions. We note that Ru^{V} species have been spectroscopically confirmed in three instances: a stable Ru^{V} complex (tetra-*n*-propylammonium bis-2-hydroxy-2-ethylbutyrato(oxo) ruthenate(V));[45] the $[Ru^{II}(bpy)_2(H_2O)_2]^{2+}$ complex oxidized by Ce^{IV};[50] and the Ru^{V},Ru^{IV} intermediate of the blue dimer.[28,29] In all three instances, at least one oxygen ligand (in addition to the Ru−H_2O fragment undergoing proton coupled electron transfer with formation of Ru^{V}=O) was present allowing for PCET and stabilization of the Ru^{V} state. The majority of single-site Ru complexes reported for water oxidation have exclusively nitrogen heterocyclic ligand environments. Such an environment is less permissive to the formation of Ru^{V} intermediates and these might become thermodynamically inaccessible. The $[Ru^{II}(bpy)(tpy)H_2O]^{2+}$ catalyst is a basic representative of such a class of catalysts. EPR, which is uniquely sensitive to the detection of the Ru^{V}=O species[49,50] even at very low concentrations (10^{11} spins per sample is a typical detection limit of EPR) failed to confirm the presence of the Ru^{V}=O species in catalytic mixtures of $[Ru^{II}(bpy)(tpy)H_2O]^{2+}$, Figure 2. Measurements in D_2O (Figure 2B) were motivated by our studies of the BD showing that Ru^{V},Ru^{IV} intermediate with Ru^{V}=O moiety can be trapped as a major species in catalytic mixtures at very early times (2−4 s) and that these times are prolonged when the reaction is carried out in D_2O.[28,29,55] No Ru^{V}=O was detected under such conditions as well as in 1 M HNO_3 used to increase redox potential of Ce^{IV} oxidant. Combined EPR and XAS analysis (Figures 2−4 and Table 1) show that under catalytic conditions the major species is $[Ru^{IV}(bpy)(tpy)=O]^{2+}$. This observation is in agreement with the ESI-MS results from the Berlinguette group.[31]

The absence of spectroscopic signatures of Ru^{IV}(OO) in the EXAFS is in agreement with ESI-MS results[31] showing less than 1% of Ru^{IV}(OO) species under catalytic steady state.

In collaboration with Prof. T. Meyer's group, we analyzed catalytic mixtures of several single-site Ru catalysts for which the Ru^{V}=O reaction with H_2O was reported to represent the rate-limiting step.[32,33] No EPR signal of Ru^{V}=O was detected in any of the studied catalysts (manuscript in preparation). Such a discrepancy is not surprising. Reliance on UV−vis kinetic analysis for the identification of the reactive intermediates has fundamental flaws in that the technique provides no direct information on the electronic or geometric structures. As a result, the reported mechanism and kinetic constant for Ru^{V}=O and O−O bond formation are highly speculative.[31−33]

An alternative mechanism has to be formulated which can account for oxygen evolution without the formation of a Ru^{V}=O species. One scenario involves the direct, but quite slow, reaction between $[Ru^{IV}(bpy)(tpy)=O]^{2+}$ and water with the formation of a peroxo intermediate. Note that redox potential of the Ru^{III}/Ru^{IV} couple in $[Ru^{II}(bpy)(tpy)H_2O]^{2+}$ is at 1.4 eV and is, thus, permissive to water oxidation (1.23 eV at pH = 0). Polyansky and collegues[24,41] characterized a distinct intermediate with an additional oxygen atom (possibly of peroxo origin) in a solution of the Ru water oxidation catalyst 4-*t*-butyl-2,6-di-1′,8′-(naphthyrid-2′-yl)-pyridine and two 4-picoline ligands subjected to bulk electrolysis below the potential assigned for the Ru^{V}=O species formation.[24] These results were used to support the reactivity of the Ru^{IV} species toward water.[24,41] Reactivity of Ru^{IV}=O with water can be envisioned as a concerted process combining either (i) first a reaction with water to form Ru^{II}−OOH and then oxidation to Ru^{III}−OOH or (ii) first oxidation to Ru^{V}=O and then its reaction with water to form Ru^{III}−OOH. Both stepwise paths will have significant barriers (Figure 6) which can be lowered by a concerted reaction in which the O−O bond is formed simultaneously with electron and proton removal. Note that the proposal of Ru^{V}=O as a distinct kinetic intermediate implies a 0.35 eV (8 kcal/mol) barrier for oxidation (using numbers from Wasylenko et al.[38]) in 0.1 M HNO_3 followed by a ∼19 kcal/mol[35] barrier predicted for the reactivity of Ru^{V}=O with water. Thus, the scenario of a distinct Ru^{V}=O kinetic intermediate seems unlikely. The Ru^{IV}=O species have a radicaloid character similar to the one established for the Ru^{V}=O species and show delocalization of the wave function to the solvent (see insert in Figure 6 with spin density picture). This interaction can provide a low overpotential pathway for O−O bond formation via a concerted mechanism. The challenge remains to engineer the catalyst−solvent interaction to increase the percentage of configurations permissive to sophisticated formation of Ru^{III}−OOH from Ru^{IV}=O with simultaneous removal of one electron and one proton. Overall, the presented results indicate a need to re-evaluate the catalyst design paradigm.

■ ASSOCIATED CONTENT

Supporting Information

Additional information on the UV−vis absorbance, EPR, analysis of the experimental EXAFS of $[Ru^{IV}(bpy)(tpy)=O]^{2+}$, $[Ru^{II}(bpy)(tpy)Cl]^{+}$ and $[Ru^{III}(bpy)(tpy)Cl]^{2+}$, and DFT computational free energies and optimized geometry of Ru intermediates. This material is available free of charge via the Internet at http://pubs.acs.org.

■ AUTHOR INFORMATION

Corresponding Author

ypushkar@purdue.edu

Present Address

[§]X-ray Science Division, Advanced Photon Source, Argonne National Laboratory, 9700 S. Cass Ave., Argonne, Illinois, 60439, United States.

Notes

The authors declare no competing financial interest.

■ ACKNOWLEDGMENTS

This work was supported by the U.S. DOE, Office of Basic Energy Sciences under grant numbers DE-FG02-10ER16184 (Y.P.) and by RFBR, research project No. 14-02-31471 (I.A.). Use of APS, an Office of Science User Facility operated by the U.S. Department of Energy (DOE) Office of Science by Argonne National Laboratory, was supported by the DOE under Contract DE-AC02-06CH11357. We thank Dr. Trudy Bolin for help with the experiments at the Beamline BM-9, APS and Dr. Steve Heald and Dr. Dale Brewe for help with experiments at Beamline BM-20, APS. We thank Dr. Ruifa Zong, Department of Chemistry at University of Houston, who provided Ru catalysts used in this work and Prof. Randolph Thummel and Prof. Tom Meyer for strong support of this study. Access to EPR was provided by the Amy Instrumentation Facility, Department of Chemistry under

the supervision of Dr. Michael Everly. We thank Prof. David McMillin for proof reading of the manuscript.

REFERENCES

(1) Gao, Y.; Ding, X.; Liu, J. H.; Wang, L.; Lu, Z. K.; Li, L.; Sun, L. C. *J. Am. Chem. Soc.* **2013**, *135* (11), 4219−4222.
(2) Zhao, Y. X.; Swierk, J. R.; Megiatto, J. D.; Sherman, B.; Youngblood, W. J.; Qin, D. D.; Lentz, D. M.; Moore, A. L.; Moore, T. A.; Gust, D.; Mallouk, T. E. *Proc. Natl. Acad. Sci. U.S.A.* **2012**, *109* (39), 15612−15616.
(3) Swierk, J. R.; Mallouk, T. E. *Chem. Soc. Rev.* **2013**, *42* (6), 2357−2387.
(4) Leung, C.-F.; Ng, S.-M.; Ko, C.-C.; Man, W.-L.; Wu, J.; Chen, L.; Lau, T.-C. *Energy Environ. Sci.* **2012**, *5* (7), 7903−7907.
(5) Berardi, S.; La Ganga, G.; Natali, M.; Bazzan, I.; Puntoriero, F.; Sartorel, A.; Scandola, F.; Campagna, S.; Bonchio, M. *J. Am. Chem. Soc.* **2012**, *134* (27), 11104−11107.
(6) Zhu, G.; Geletii, Y. V.; Koegerler, P.; Schilder, H.; Song, J.; Lense, S.; Zhao, C.; Hardcastle, K. I.; Musaev, D. G.; Hill, C. L. *Dalton Trans.* **2012**, *41* (7), 2084−2090.
(7) McCool, N. S.; Robinson, D. M.; Sheats, J. E.; Dismukes, G. C. *J. Am. Chem. Soc.* **2011**, *133* (30), 11446−11449.
(8) Dogutan, D. K.; McGuire, R., Jr.; Nocera, D. G. *J. Am. Chem. Soc.* **2011**, *133* (24), 9178−9180.
(9) McDaniel, N. D.; Coughlin, F. J.; Tinker, L. L.; Bernhard, S. *J. Am. Chem. Soc.* **2008**, *130* (1), 210−217.
(10) Hull, J. F.; Balcells, D.; Blakemore, J. D.; Incarvito, C. D.; Eisenstein, O.; Brudvig, G. W.; Crabtree, R. H. *J. Am. Chem. Soc.* **2009**, *131* (25), 8730−8731.
(11) Blakemore, J. D.; Schley, N. D.; Balcells, D.; Hull, J. F.; Olack, G. W.; Incarvito, C. D.; Eisenstein, O.; Brudvig, G. W.; Crabtree, R. H. *J. Am. Chem. Soc.* **2010**, *132* (45), 16017−16029.
(12) Fillol, J. L.; Codola, Z.; Garcia-Bosch, I.; Gomez, L.; Pla, J. J.; Costas, M. *Nat. Chem.* **2011**, *3* (10), 807−813.
(13) Wasylenko, D. J.; Palmer, R. D.; Berlinguette, C. P. *Chem. Commun.* **2013**, *49* (3), 218−227.
(14) Singh, A.; Spiccia, L. *Coord. Chem. Rev.* **2013**, *257* (17−18), 2607−2622.
(15) Gersten, S. W.; Samuels, G. J.; Meyer, T. J. *J. Am. Chem. Soc.* **1982**, *104* (14), 4029−4030.
(16) Wada, T.; Tsuge, K.; Tanaka, K. *Angew. Chem., Int. Ed.* **2000**, *39* (8), 1479−1482.
(17) Deng, Z. P.; Tseng, H. W.; Zong, R. F.; Wang, D.; Thummel, R. *Inorg. Chem.* **2008**, *47* (6), 1835−1848.
(18) Zong, R.; Thummel, R. *J. Am. Chem. Soc.* **2005**, *127* (37), 12802−12803.
(19) Concepcion, J. J.; Jurss, J. W.; Templeton, J. L.; Meyer, T. J. *J. Am. Chem. Soc.* **2008**, *130* (49), 16462−16463.
(20) Kaveevivitchai, N.; Zong, R. F.; Tseng, H. W.; Chitta, R.; Thummel, R. P. *Inorg. Chem.* **2012**, *51* (5), 2930−2939.
(21) Hirahara, M.; Ertem, M. Z.; Komi, M.; Yamazaki, H.; Cramer, C. J.; Yagi, M. *Inorg. Chem.* **2013**, *52* (11), 6354−6364.
(22) Yagi, M.; Tajima, S.; Komi, M.; Yamazaki, H. *Dalton Trans.* **2011**, *40* (15), 3802−3804.
(23) Yamazaki, H.; Hakamata, T.; Komi, M.; Yagi, M. *J. Am. Chem. Soc.* **2011**, *133* (23), 8846−8849.
(24) Polyansky, D. E.; Muckerman, J. T.; Rochford, J.; Zong, R.; Thummel, R. P.; Fujita, E. *J. Am. Chem. Soc.* **2011**, *133* (37), 14649−14665.
(25) Duan, L. L.; Bozoglian, F.; Mandal, S.; Stewart, B.; Privalov, T.; Llobet, A.; Sun, L. C. *Nat. Chem.* **2012**, *4* (5), 418−423.
(26) Yamada, H.; Siems, W. F.; Koike, T.; Hurst, J. K. *J. Am. Chem. Soc.* **2004**, *126* (31), 9786−9795.
(27) Cape, J. L.; Lymar, S. V.; Lightbody, T.; Hurst, J. K. *Inorg. Chem.* **2009**, *48* (10), 4400−4410.
(28) Moonshiram, D.; Jurss, J. W.; Concepcion, J. J.; Zakharova, T.; Alperovich, I.; Meyer, T. J.; Pushkar, Y. *J. Am. Chem. Soc.* **2012**, *134* (10), 4625−4636.
(29) Moonshiram, D.; Alperovich, I.; Concepcion, J. J.; Meyer, T. J.; Pushkar, Y. *Proc. Natl. Acad. Sci. U.S.A.* **2013**, *110* (10), 3765−3770.
(30) Stull, J. A.; Stich, T. A.; Hurst, J. K.; Britt, R. D. *Inorg. Chem.* **2013**, *52* (8), 4578−4586.
(31) Wasylenko, D. J.; Ganesamoorthy, C.; Henderson, M. A.; Koivisto, B. D.; Osthoff, H. D.; Berlinguette, C. P. *J. Am. Chem. Soc.* **2010**, *132* (45), 16094−16106.
(32) Concepcion, J. J.; Tsai, M. K.; Muckerman, J. T.; Meyer, T. J. *J. Am. Chem. Soc.* **2010**, *132* (5), 1545−1557.
(33) Concepcion, J. J.; Jurss, J. W.; Norris, M. R.; Chen, Z. F.; Templeton, J. L.; Meyer, T. J. *Inorg. Chem.* **2010**, *49* (4), 1277−1279.
(34) Wang, L.-P.; Wu, Q.; Van Voorhis, T. *Inorg. Chem.* **2010**, *49* (10), 4543−4553.
(35) Hughes, T. F.; Friesner, R. A. *J. Phys. Chem. B* **2011**, *115* (29), 9280−9289.
(36) Masaoka, S.; Sakai, K. *Chem. Lett.* **2009**, *38* (2), 182−183.
(37) Vigara, L.; Ertem, M. Z.; Planas, N.; Bozoglian, F.; Leidel, N.; Dau, H.; Haumann, M.; Gagliardi, L.; Cramer, C. J.; Llobet, A. *Chem. Sci.* **2012**, *3* (8), 2576−2586.
(38) Wasylenko, D. J.; Ganesamoorthy, C.; Henderson, M. A.; Berlinguette, C. P. *Inorg. Chem.* **2011**, *50* (8), 3662−3672.
(39) Tseng, H. W.; Zong, R.; Muckerman, J. T.; Thummel, R. *Inorg. Chem.* **2008**, *47* (24), 11763−11773.
(40) Boyer, J. L.; Polyansky, D. E.; Szalda, D. J.; Zong, R. F.; Thummel, R. P.; Fujita, E. *Angew. Chem., Int. Ed.* **2011**, *50* (52), 12600−12604.
(41) Badiei, Y. M.; Polyansky, D. E.; Muckerman, J. T.; Szalda, D. J.; Haberdar, R.; Zong, R.; Thummel, R. P.; Fujita, E. *Inorg. Chem.* **2013**, *52* (15), 8845−8850.
(42) Concepcion, J. J.; Binstead, R. A.; Alibabaei, L.; Meyer, T. J. *Inorg. Chem.* **2013**, *52* (19), 10744−10746.
(43) Takeuchi, K. J.; Thompson, M. S.; Pipes, D. W.; Meyer, T. J. *Inorg. Chem.* **1984**, *23* (13), 1845−1851.
(44) Kaveevivitchai, N.; Chitta, R.; Zong, R. F.; El Ojaimi, M.; Thummel, R. P. *J. Am. Chem. Soc.* **2012**, *134* (26), 10721−10724.
(45) Dengel, A. C.; Griffith, W. P.; O'Mahoney, C. A.; Williams, D. J. *J. Chem. Soc.-Chem. Commun.* **1989**, *22*, 1720−1721.
(46) Godbout, N.; Salahub, D. R.; Andzelm, J.; Wimmer, E. *Can. J. Chem.* **1992**, *70* (2), 560−571.
(47) Velde, G. T.; Bickelhaupt, F. M.; Baerends, E. J.; Guerra, C. F.; Van Gisbergen, S. J. A.; Snijders, J. G.; Ziegler, T. *J. Comput. Chem.* **2001**, *22* (9), 931−967.
(48) Lachancegalang, K. J.; Doan, P. E.; Clarke, M. J.; Rao, U.; Yamano, A.; Hoffman, B. M. *J. Am. Chem. Soc.* **1995**, *117* (12), 3529−3538.
(49) Dengel, A. C.; Griffith, W. P. *Inorg. Chem.* **1991**, *30* (4), 869−871.
(50) Planas, N.; Vigara, L.; Cady, C.; Miro, P.; Huang, P.; Hammarstrom, L.; Styring, S.; Leidel, N.; Dau, H.; Haumann, M.; Gagliardi, L.; Cramer, C. J.; Llobet, A. *Inorg. Chem.* **2011**, *50* (21), 11134−11142.
(51) Taketoshi, A.; Koizumi, T.-A.; Kanbara, T. *Tetrahedron Lett.* **2010**, *51* (49), 6457−6459.
(52) Dobson, J. C.; Meyer, T. J. *Inorg. Chem.* **1988**, *27* (19), 3283−3291.
(53) Sala, X.; Ertem, M. Z.; Vigara, L.; Todorova, T. K.; Chen, W. Z.; Rocha, R. C.; Aquilante, F.; Cramer, C. J.; Gagliardi, L.; Llobet, A. *Angew. Chem., Int. Ed.* **2010**, *49* (42), 7745−7747.
(54) Wasylenko, D. J.; Ganesamoorthy, C.; Koivisto, B. D.; Henderson, M. A.; Berlinguette, C. P. *Inorg. Chem.* **2010**, *49* (5), 2202−2209.
(55) Moonshiram, D.; Purohit, V.; Concepcion, J. J.; Meyer, T. J.; Pushkar, Y. *Materials* **2013**, *6* (2), 392−409.